47th SME North American Manufacturing Research Conference, Penn State Behrend Erie, Pennsylvania, 2019

Assessment of the Mechanical Integrity of a 2 mm AA6060-T6 Butt Weld Produced Using the Hybrid Metal Extrusion & Bonding (HYB) Process – Part I: Bend Test Results

Lise Sandnes[a],*, Luca Romere[b], Filippo Berto[a], Torgeir Welo[a], Øystein Grong[a,c]

[a]*Department of Mechanical and Industrial Engineering, Norwegian University of Science and Technology, Richard Birkelands vei 2b, 7491 Trondheim, Norway*
[b]*Department of Management and Engineering, University of Padua, Stradella San Nicola 3, 36100 Vicenza, Italy*
[c]*HyBond AS, NAPIC, Richard Birkelands vei 2b, 7491 Trondheim Norway*

* Corresponding author. Tel.: + 47 924 66 968. *E-mail address:* Lise.Sandnes@ntnu.no

Abstract

The present investigation is concerned with butt welding of 2 mm thin AA6060-T6 profiles at room temperature (RT), using the HYB process and AA6082-T4 as filler material. In the as-welded condition, the 1000 mm long butt weld is seen to be straight and free from global distortions. At the same time both weld faces appear slick and display a nice surface finish. However, cold flow results in the formation of internal voids in the beginning of the weld, but these defects gradually disappear as the temperature distribution approaches pseudo-steady state further ahead. Still, root cracks evolved during instrumented three-point bend testing along the entire length of the weld because of "kissing" bond formation. Based on ABAQUS simulations of the bend test it is concluded that they form when the plastic tensile strain component on the root side of the weld exceeds about 0.38. Hence, the "kissing" bond formation is not devastating for the resulting mechanical integrity of the joint.

1. Introduction

Al-Mg-Si alloys are to an increasing extent used for structural applications within the transportation and automotive sector by virtue of their high strength, excellent formability, low weight and good resistance to general corrosion [1, 2]. In load-bearing structures the solute-rich AA6082 and AA6061 variants are most commonly employed, since they provide the highest specific strength (i.e. yield strength to density ratio) in the peak-aged (T6) temper condition [3]. However, problems arise when these alloys following peak-ageing are subjected to welding, as frequently done in industrial manufacturing of aluminum components [1, 4]. This is because T6 heat-treated Al-Mg-Si alloys are particularly prone to heat-affected zone (HAZ) softening after gas metal arc welding (GMAW) and friction stir welding (FSW), which reduces the load-bearing

capacity of the entire assembly [5, 6]. In addition, welding of thin section aluminum plates and profiles creates additional problems related to buckling and global distortions [7, 8]. These problems are most severe in GMAW, but can be reduced by the use of an energy efficient solid state process like FSW [9-11]. Still, buckling and distortions represent a great challenge for many manufacturers of aluminum parts, who daily face the strict dimensional tolerance requirements being enforced by their customers.

No simple actions can be undertaken to counteract the negative effects of welding for thin section products. But a bold, new approach could be to instead select a lean aluminum alloy (e.g. of the 6060-T6 type), and employ this, in combination with solid state joining, for manufacturing of such products. The use of an aluminum alloy with a low base metal (BM) strength will inevitably reduce the significance of the

HAZ softening. This is because the drop in strength following dissolution of the BM hardening precipitates will be correspondingly small. However, since FSW of thin plates may result in insufficient material feeding and consequently to undercuts and weld defects [12, 13], an alternative solid state process enabling filler metal addition should be aimed at. If the resulting mechanical properties and dimensional tolerances achieved in the as-welded condition are better than those obtained following GMAW and FSW of the high strength AA6082-T6 and AA6061-T6 variants, the approach is deemed to be viable and sound. This is the key research question that will be answered in the present investigation.

Recently, it has been documented that the Hybrid Metal Extrusion & Bonding (HYB) process can produce sound 4 mm thick AA6082-T6 butt welds using AA6082 filler metal additions with properties matching those of corresponding GMA and FS weldments [14]. Because the energy efficiency of the HYB method is comparable with that of FSW when it comes to heat input and extent of HAZ softening, this process should be an excellent candidate for butt welding of 2 mm thin AA6060-T6 extrusions. To meet the customer's dimensional tolerance requirements for manufacturing of wide profiles from narrow-width extrusions both weld surfaces need to be slick as in FSW, without a reinforcement. At the same time as the joined profiles must be straight and display a nice surface finish in the as-welded condition.

In Part I of this investigation the results from the visual inspection, macroscopic examination and instrumented three-point bend testing of the weld are presented. The bend test has been chosen because it allows easy detection of possible surface and root defects that can affect the mechanical integrity of the joint. The resulting tensile and fatigue test results are then reported in two accompanying papers (Part II and III, respectively).

2. Experimental

The working principles of the HYB PinPoint extruder and its ability to handle different joint configurations and weld geometries as well as base metal combinations have been reported elsewhere [14, 15]. For the 2 mm butt welding application, a stationary housing with no die opening at the rear for partial outlet of the extrudate is selected to prevent the formation of a reinforcement. When this closed housing is used in combination with a flat steel backing plate, a slick weld and root face can be obtained also in the HYB case as in FSW.

2.1. Materials and welding conditions

The 2 mm thin AA6060 extrusions used in the butt joining trial were received from an external supplier in the T6 temper condition. The other dimensions of the extrusions were 50 mm × 1000 mm. The filler material was a $\phi 1.2$ mm wire of the AA6082-T4 type produced by HyBond AS. The wire was made from a $\phi 95$ mm DC cast billet which then was homogenized, hot extruded, cold drawn and shaved down to the final dimension. The chemical compositions of the base and filler materials (BM and FM) are summarized in Table 1.

Prior to the welding operation, the two 1000 mm long extruded profiles were mounted in a fixture so that a 7.5 mm wide I-groove did form between them, as illustrated in Fig. 1 (a). During butt welding the extruder head with its $\phi 9$ mm rotating cylindrical pin slides at a constant speed along the 7.5 mm wide I-groove, as shown in Fig. 1 (b). Due to the synchronized spindle tip and pin rotation, the $\phi 1.2$ mm filler wire is continuously dragged by friction into and through the extrusion chamber. When it hits the abutment, the subsequent compression and pressure build-up eventually lead to extrusion of the plasticized aluminum in the axial direction through a set of moving dies in the rotating pin and downwards into the groove [14, 15]. Because the pin diameter is larger than the groove width, the surface oxide being present at the groove walls becomes continuously mixed into the filler metal (FM) before bonding and consolidation occur behind the pin.

Table 2 summarizes the operational conditions employed in the butt welding experiment. Note that the current combination of welding parameters used is not considered to be optimal, but represent rather a sensible compromise between a number of conflicting requirements to achieve a weld with the required groove filling and surface finish. A more in-depth analysis of the essential HYB process parameters and how they are interrelated are provided in Ref. [15].

Table 1. Chemical compositions (wt.%) of the base and filler materials (BM and FM).

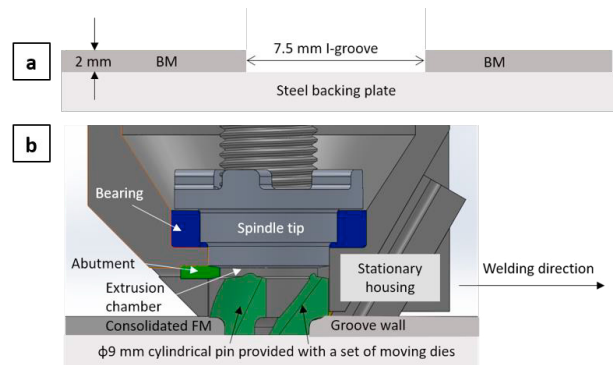|	Si	Mg	Fe	Mn	Ti	Other	Al
BM	0.483	0.435	0.176	0.038	0.021	0.114	Balance
FM	1.110	0.610	0.200	0.510	0.043	0.278	Balance

Fig. 1. Schematic and SolidWorks drawings highlighting the experimental set-up during butt welding of the 2 mm thin AA6060-T6 extruded profiles; (a) Transverse section showing the groove and base plate dimensions. (b) Longitudinal section through the extruder head and the weld with the rotating cylindrical pin in position within the groove and the closed stationary housing placed on the top.

Table 2. Operational conditions employed in the butt welding experiment with the 2 mm thin extruded profiles.

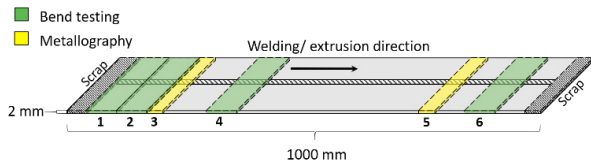| Pin rotation (RPM)	Travel speed (mm/s)	Wire feed rate (mm/s)	Gross heat input (kJ/mm)
250	8	122	0.28

Fig. 2. Sketch showing the location of the different samples used for metallography (yellow) and bend testing (green) referred to the start position of the weld.

2.2. Visual inspection and metallographic examination

After the butt welding operation the joined profiles were gently released from the fixture and pictures taken at low magnification to document their as-welded straightness and surface quality. In addition, cross sectional samples were cut from the weld at two different locations and made ready for metallographic examination using standard preparation techniques. The location of these samples, referred to the start position of the weld, is illustrated in Fig. 2.

To reveal the macrostructure of the weld the samples were first leached in a solution of 1 g NaOH per 100 ml H_2O for 3 to 4 minutes. Then they were examined in an Alicona Confocal microscope at different magnifications for documentation of the FM and BM flow patterns and detection of possible weld defects and cracks in the bend-tested samples.

2.3. Instrumented three-point bend testing

The instrumented three-point bend testing was conducted in accordance to ASTM standard 290-14 [16] (which applies to plate materials) because this standard also allows testing of sub-size samples. The number of transverse sub-size specimens being extracted from the weld and their locations referred to the start position of the weld are highlighted in Fig. 2. Note that these sub-size specimens have the same length-to-width ratio as specimens commonly used for bend testing of weld ductility (i.e. ASTM standard E190-14 [17]), although their width-to-thickness ratio is slightly smaller than that allowed for in the standard. Hence, the shear stress to normal stress ratio in the sub-size specimens is similar to that in the weld ductility specimens (i.e. close to 0.05 in both cases). The latter has been verified using ABAQUS simulations of both specimen types.

Fig. 3 shows a drawing of the bend test experimental set-up and the dimensions of the sub-size specimens used in the experiments, Table 3 provides further details of the number and type of specimens being tested. Note that the two specimens used for sampling the base material ductility were extracted from a separate extrusion. The experimental three-point bend tests were conducted at a constant force velocity of 1 mm/min.
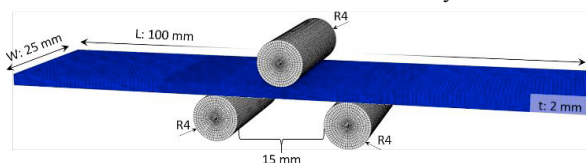

Fig. 3. Drawing showing the experimental set-up and the dimensions of the sub-size weld specimens being used in the bend testing trials.

Lubricant was used in order to reduce the friction between the workpiece and the tools. All weld specimens were bent to an angle of 180 degrees, whereas the two base material specimens were bent to an angle of 90 degrees due to their shorter length being limited by the width of the BM extrusions.

Table 3. Overview of the type of specimens being used in three-point testing. The numbering is in accordance with the labelling used in Fig. 2. Note that specimens used for bend testing of the base material were extracted from a separate extrusion.

Region tested	Specimen No.	Comments
Weld face	1, 6	Extracted from the weld
Weld root	2, 4	Extracted from the weld
Base material	7, 8	Extracted from a separate extrusion

2.4. Finite element analysis

Simulations of the three-point bend test were conducted using the commercial finite element (FE) software code ABAQUS/CAE (6.17) [18]. The modelled surface of the tool and the workpiece are exact physical representations of the experimental setup. In the simulations, the tools (shoulders and plunger) are modelled as rigid objects, while the aluminium workpiece is modelled as a deformable object and represented by a solid mesh of approximately 90 000 quadratic brick elements (C3D20R). A finer mesh was chosen for its mid-section where the workpiece is in physical contact with the tools and extensive plastic deformation of the workpiece occurs. The number of elements in the workpiece thickness direction was set to 8 after conducting a mesh sensitivity analysis. Hence, mesh refinement above this point does not affect the resulting output data significantly.

In order to obtain a highest possible accuracy in the simulations relevant material in-put data must be used. These data are based on the tensile test results of the base material, which are reported in Part II of this investigation. The friction coefficient is set to 0.12, which is a reasonable value in metal forming operations involving the use of lubricants and aluminium-steel interaction [19, 20].

3. Results

3.1. As-welded joint quality and surface finish

After the welding operation low magnification pictures were taken in order to document the as-welded joint quality and
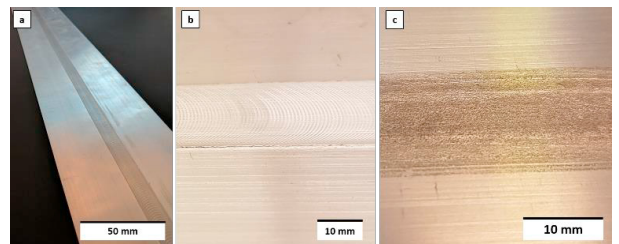

Fig. 4. Photographs of the 2 mm AA6060-T6 HYB butt joint; (a) Overview of as-welded profile, (b) Close-up of weld face, (c) Close-up of weld root.
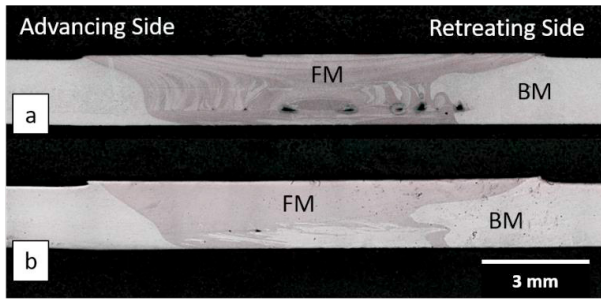
Fig. 5. Optical macrographs of the transverse cross-section at two different locations along the weld; (a) Start position, (b) Central part of weld.

surface finish. Fig. 4 (a) shows an overview of the 1000 mm long weld, which appears to be straight and free from global distortions. Moreover, both the weld face and root have a slick surface, as can be seen from the close-up pictures in Fig. 4 (b) and (c), respectively. Still, the weld face is approximately 0.2 mm above the BM surface due to the filler material addition.

Optical micrographs of the weld cross section at two different locations along the weld are presented in Fig. 5, from which the BM and FM flow patterns also can be seen. In the weld start region (Fig. 5 (a)), insufficient material flow results in internal void formation. These voids are located approximately 0.4 mm above the weld root and are between 0.04 and 0.43 mm in size. However, in the central part of the weld (Fig. 5 (b)) the joint appears to be essentially free from internal defects, indicating that the material flow in this case has been sufficient vigorous to promote adequate mixing and stirring of the base and filler materials.

3.2. Bend test results

The purpose of the three-point bend testing is to disclose weld defects and "kissing" bond formation, which are difficult to detect by other means. The main results from the instrumented bend testing are graphically presented in Fig. 6. In Fig. 6 (a), the two BM force-displacement curves are shown. Figs. 6 (b) and (c) show the corresponding curves for the weld face and the weld root specimens, respectively, along with the BM curve No. 7, which serves as a reference for the other ones. It follows from the latter graphs that specimens extracted from the weld start region reach a slightly lower maximum force compared to those located in the central part and at the end of the weld. Moreover, it appears that the peak force is highest for the weld face specimens and somewhat lower for the weld root specimens. Furthermore, a closer inspection of Fig. 6 (c) reveals a sharp break in the force-displacement curve at about 12 mm for weld root specimen No. 2. Otherwise, the curves closely resemble those obtained for the BM being presented in Fig. 6 (a), reaching the maximum force after a displacement of about 7 mm.

3.3. Crack formation in bend-test samples

After the instrumented three-point bend testing all specimens were visually examined. Both the base material and the weld face specimens did pass the bend test. This means that no cracks could be observed on the outer convex of the

specimens. In contrast, a longitudinal surface crack appears in the two weld root specimens after a displacement of about 11 mm. This is shown in Fig. 7. As can be seen from the figure, the crack formation is most distinct for the specimen located in the weld start region (Fig. 7 (a)) and less apparent for the specimen extracted from the central part of the weld (Fig. 7
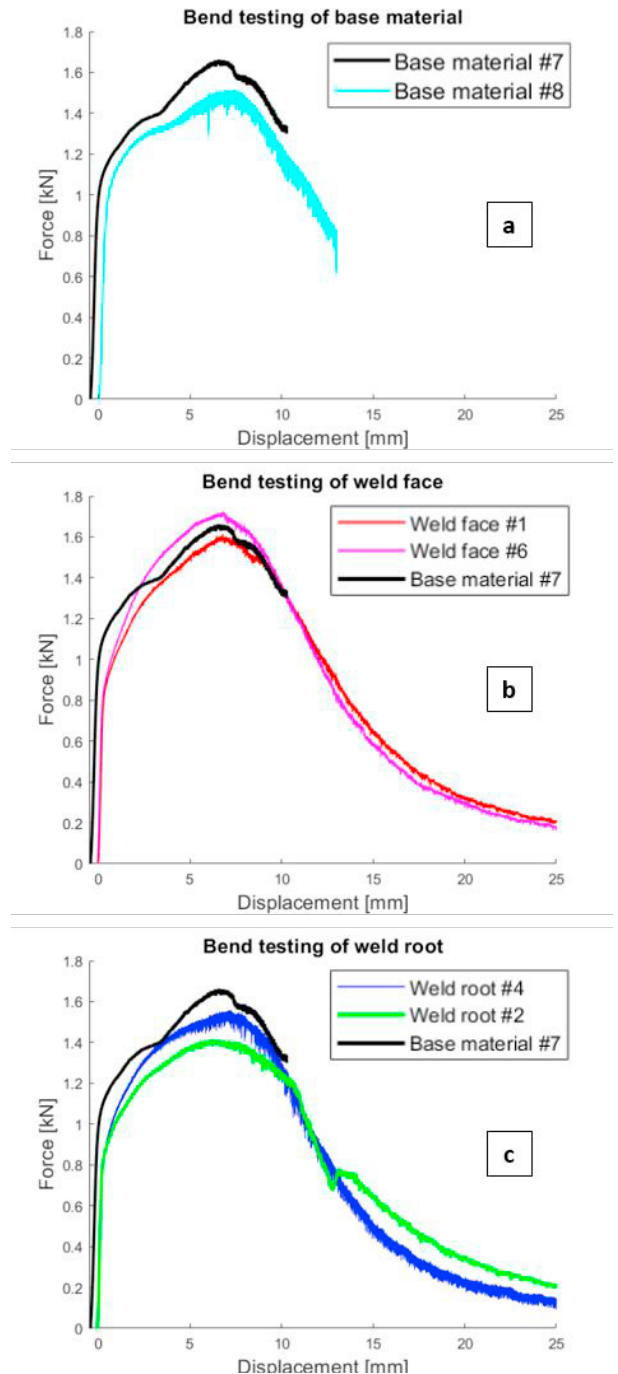

Fig. 6. Measured force-displacement curves for the different bend test samples; (a) Base material, (b) Weld face, (c) Weld root. The specimen labelling and numbering are in accordance with Fig. 2 and Table 3, respectively. Note that the curve for base material specimen Nr. 7 is also included in figures (b) and (c) for comparison.
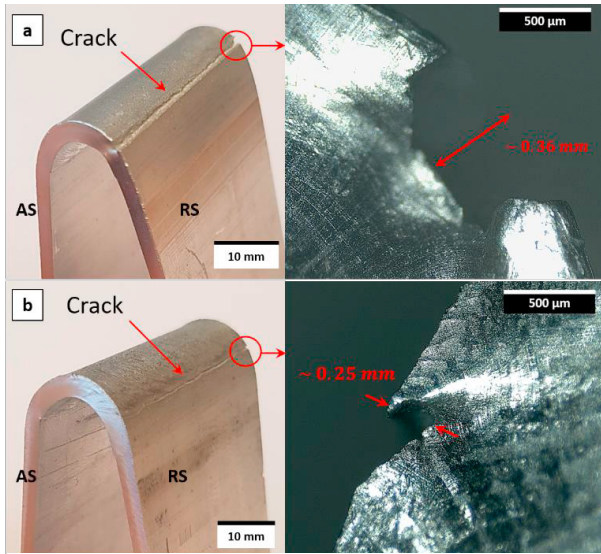
Fig. 7. Photographs of the weld root specimens along with close-ups of the root cracks detected on the retreating side of the weld following bend testing; (a) Start region of weld, (b) Central part of weld.
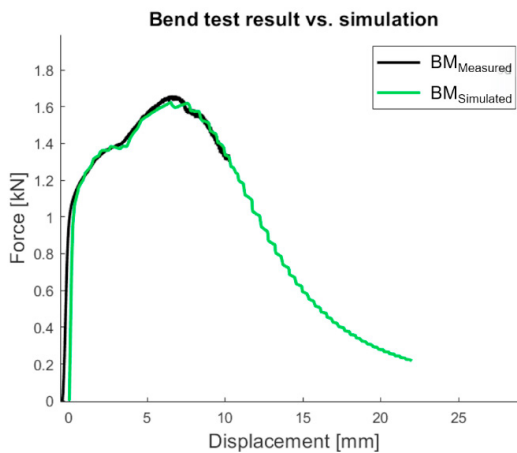

Fig. 8. Simulated (green) and measured (black) force-displacement curves for the AA6060-T6 base material during three-point bend testing.

(b)). In these specimens the measured crack depth is 0.36 and 0.25 mm, respectively.

4. Discussion

4.1. Finite element analysis of the three-point bend test

The deformation pattern and plastic strain development in the specimens during three-point bend testing have been evaluated by means of finite element (FE) simulations of the base material. The simulated force-displacement curve (green curve) is shown in Fig. 8, along with the corresponding measured curve for the AA6060-T6 base material (black curve). As can be seen from these plots, the FE model gives a very good representation of the BM deformation pattern during three-point bend testing. Because the measured force-displacement curves for the weld specimens do not depart

significantly from the base metal curve (see Fig. 6), it is reasonable to assume that the FE model also gives a fair representation of the deformation pattern in the former specimens.

In three-point bend testing the workpiece is subjected to extensive plastic deformation, leading to large plastic strains in the material. Table 4 summarizes the plastic tensile strain development (ε_{p11}) in the longitudinal center point of the convex bend at different displacements. Note that the positive and negative values for the strain refer to the outer and inner radius of the bend, respectively. It follows that the maximum plastic tensile strain is obtained at a displacement of about 9 mm. The strain then saturates at a value of ±0.38. Fig. 9 shows the corresponding plastic tensile strain distribution within the entire workpiece at saturation.

In view of the large plastic tensile strains that the bend test specimens are exposed to before root cracking occurs, it is concluded that the mechanical integrity of the HYB weld is sufficiently high to justify further tensile and fatigue testing, as planned for in Part II and III of the investigation.

Table 4. Calculated plastic tensile strains occurring in the longitudinal center point of the workpiece convex bend at different displacements during three-point bend testing.

Displacement (mm)	Plastic Strain (ε_{p11})	Comments
5	±0.30	
7	±0.36	Maximum force is reached
9	±0.38	Maximum plastic strain is reached
25	±0.38	

4.2. Origin of the root crack problem

From Fig. 7 it is evident that root cracks form on the retreating side of the joint in the weld root specimens during three-point bend testing. Moreover, the largest cracks appear in
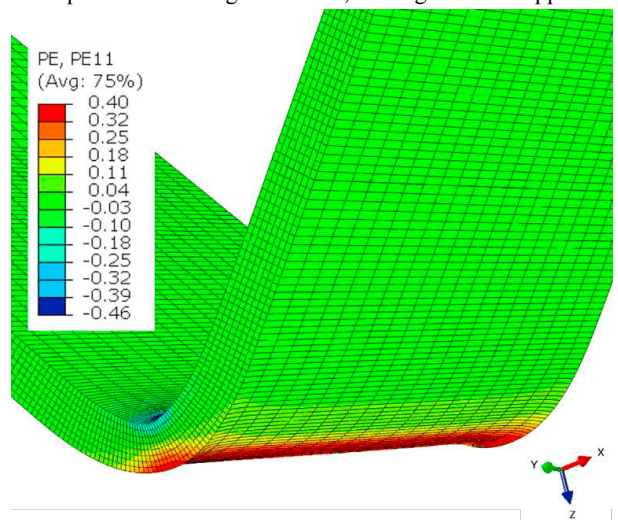

Fig. 9. ABAQUS snapshot showing the plastic tensile strain distribution within the entire workpiece following bend testing at a displacement of 9 mm. Included is also a colour bar in the upper left corner showing the corresponding plastic tensile strain values.

the beginning of the weld, whereas more shallow cracks form in the central part of the weld. In order to understand the origin of this cracking phenomenon, a microscopic examination of the weld root region has been conducted.

Fig. 10 (a) and (b) show close-ups of the weld root region on the advancing and retreating side of the joint, respectively. As can be seen, the bond line appears different in the two figures. On the advancing side of the joint, there is a smooth transition between the base and filler materials, whereas on the retreating side, the bond line is sharp for about 0.18 mm before it starts to become blurred. The same is also true for the specimen located closer to the weld end (see Fig. 11), although the bond line length in this case is somewhat shorter. The presence of a sharp bond line in the root region of the weld on the retreating side is a strong indication of "kissing" bond formation. This phenomenon has its origin in oxide accumulation at the FM-BM interface, leading cracking during subsequent bend testing. "Kissing" bond formation is a well-known problem also in FSW of aluminum alloys, and has been the subject of many investigations in the past [21-24].
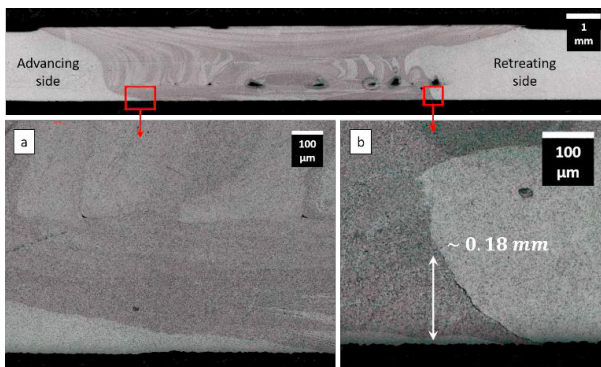

Fig. 10. Micrographs highlighting the root region in the start position of the weld; (a) Close-up of the bond line on the advancing side of the joint, (b) Close-up of the bond line on the retreating side of the joint.
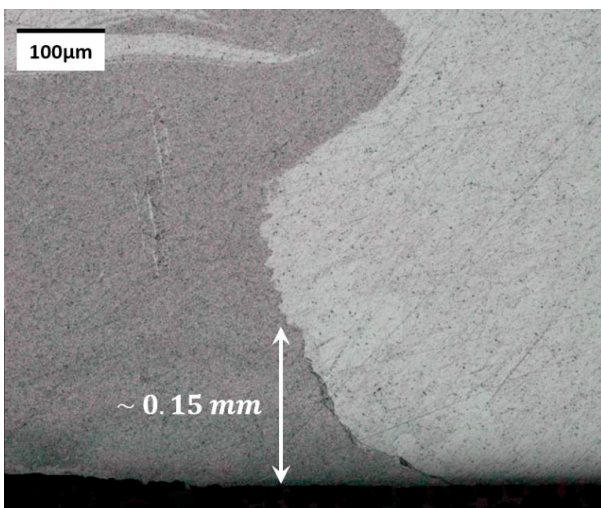

Fig. 11. Close-up of the root region at a position nearer to the end of the weld.

4.3. Origin of the cold flow phenomenon

As shown previously in Fig. 5, internal void formation due to cold flow is most pronounced in the beginning of the weld. This observation is not surprising, considering the fact that the duration of the transient heating period is quite long during thin plate aluminum welding. Typically, the temperature within the weld region will continue to increase the first 75 to 100 mm after start-up before pseudo-steady state is reached [4]. Furthermore, the massive steel backing plate used in the HYB welding trial will also act as an effective heat sink under the prevailing circumstances. Both factors contribute significantly to the observed cold flow phenomenon and the internal void formation, particularly in the start position of the weld.

5. Conclusions

It is confirmed that the HYB process can be used for butt welding of 2 mm thin AA6060-T6 profiles in the solid-state using filler metal addition.

The HYB butt weld meets the strict quality requirements being specified for the product when it comes to straightness and surface finish in the as-welded condition. This means that the HYB PinPoint extruder is able to fill the 7.5 mm wide I-groove separating the profiles with AA6082-T4 extrudate in one pass without contributing to global distortions or formation of a weld reinforcement.

The central part of the butt weld is found to be essentially free from internal defects like pores and voids. However, cold flow results in the formation of voids in the beginning of the weld before the temperature in the root region reaches pseudo-steady state.

Finally, an ABAQUS finite element model has been developed and used to simulate the weld bend testing. Following calibration of the model and benchmarking against the base metal bend test results, it is concluded that the root cracks start to form when the plastic tensile strain component on the root face approaches 0.38. Hence, the detected "kissing" bond formation in the root region on the retreating side of the weld is not devastating for the resulting mechanical integrity. This justifies further tensile and fatigue testing of the HYB joint, as planned for in Part II and III of the investigation.

References

[1] Hirsch J. Aluminium in innovative light-weight car design. Mater. Trans. 2011;52:818-824.
[2] Davis JR. Aluminum and aluminum alloys. Materials Park, US, 1993.
[3] Hatch JE. Aluminum – properties and physical metallurgy. Materials Park, US, 1984.

[4] Grong Ø. Metallurgical modelling of welding. 2nd ed. London, UK, 1997.

[5] Myhr OR, Grong Ø. Novell modelling approach to optimisation of welding condition and heat treatment schedules for age hardening Al alloys. Sci. Technol. Weld. Joining 2009;14:321-332.

[6] Frigaard Ø, Grong Ø, Midling OT. A process model for friction stir welding of age hardened aluminium alloys. Metall. Mater. Trans. A 2001;32:1189-1200.

[7] Bruce GJ, Eyres DJ. Ship construction. 7th ed. Oxford, UK, 2012.

[8] Zha Y, T Moan. Ultimate strength of stiffened aluminium panels with predominantly torsional failure mode. Thin Wall. Struct. 2001;39:631-648.

[9] Kumar R, et al. Welding of thin sheet of Al alloy (6082) by using Vario wire DC P-GMAW. Int. J. Adv. Manuf. Technol. 2008;42:102-117.

[10] Farajkhah V, Liu Y, Gannon L. Finite element stud of 3D simulated welding effect in aluminium plates. Ships and Offshore Struc. 2017;12:196-208.

[11] Ma ZY, et al. Recent advances in friction stir welding/processing of aluminium alloys: microstructural evolution and mechanical properties. Crit. Rev. Solid State Mater. Sci. 2018;43:269-333.

[12] Wanjara P, Monsarrat B, Larose S. Gap tolerance allowance and robotic operational window for friction stir butt welding of AA6061. J. Mater. Process. Technol. 2013;213:631-640.

[13] Huang Y, et al. The weld formation of self-support friction stir welds of aluminium hollow extrusions. Int. J. Adv. Manuf. Technol. 2016;87:1067-1075.

[14] Sandnes L, et al. Exploring the hybrid metal extrusion & bonding process for butt welding of Al-Mg-Si alloys. Int. J. Adv. Manuf. Technol. 2018; 98:1059-1065.

[15] Grong Ø, Sandnes L, Berto F. A status report on the Hybrid Metal Extrusion & Bonding (HYB) process and its application. Materials Design and Processing Communication (In press).

[16] ASTM Standard. Standard test method for bend testing of material ductility 290-14. ASTM international, 2014.

[17] ASTM Standard. Standard test method for guided bend test for ductility of welds E190-14. ASTM international. 2014.

[18] Dasult Systems SIMULIA Corp. ABAQUS/CAE (Version 6.17). Johnston, USA.

[19] Lilleby A, et al. Experimental and finite element studies of the divergent extrusion process under conditions applicable to cold pressure welding of commercial purity aluminium. Mater. Sci. Eng. A 2009;518:76-83.

[20] Valberg HS. Applied metal forming. London, UK, 2010.

[21] Saro YS, et al. Characteristics of the kissing-bond in friction stir welded Al alloy 1050. Mater. Sci. Eng. A 2005;405:333-338.

[22] Oosterkamp A, Oosterkamp LD, Nordeide A. 'Kissing bond' penomena in solid-state welds of aluminium alloys. Weld. J. (NY, United States), 2004;83:225-231.

[23] Kadlec M, Ruzek R, Nováková L. Mechanical behaviour of AA7475 friction stir welds with the kissing bond defect. Int. J. Fatigue 2015;74:7-19.

[24] Li B, Shen Y, Hu W. The study on defects in aluminu 2219-T6 thick butt friction stir welds with the application of multiple non-destructive testing methods. Mater. Des. 2011;32:2073-2084.